Strong enhancement of light absorption and highly directive thermal emission in graphene

Mingbo Pu,[1] Po Chen,[2] Yanqin Wang,[1] Zeyu Zhao,[1] Changtao Wang,[1] Cheng Huang,[1] Chenggang Hu,[1] and Xiangang Luo[1,*]

[1]*State Key Laboratory of Optical Technologies on Nano-Fabrication and Micro-Engineering, Institute of Optics and Electronics, Chinese Academy of Science, P.O. Box 350, Chengdu 610209, China*
[2]*Department of Geology and Geophysics, University of Wyoming, Laramie, Wyoming 82071, USA*
[*] *lxg@ioe.ac.cn*

Abstract: Graphene is a two-dimensional material with exotic electronic, optical and thermal properties. The optical absorption in monolayer graphene is limited by the fine structure constant α. Here we demonstrated the strong enhancement of light absorption and thermal radiation in homogeneous graphene. Numerical simulations show that the light absorbance can be controlled from near zero to 100% by tuning the Fermi energy. Moreover, a set of periodically located absorption peaks is observed at near grazing incidence. Based on this unique property, highly directive comb-like thermal radiation at near-infrared frequencies is demonstrated.

OCIS codes: (160.3918) Metamaterials; (290.6815) Thermal emission; (310.3915) Metallic, opaque, and absorbing coatings.

References and links

1. K. S. Novoselov, A. K. Geim, S. V. Morozov, D. Jiang, M. I. Katsnelson, I. V. Grigorieva, S. V. Dubonos, and A. A. Firsov, "Two-dimensional gas of massless Dirac fermions in graphene," Nature **438**(7065), 197–200 (2005).
2. Y. Zhang, Y. W. Tan, H. L. Stormer, and P. Kim, "Experimental observation of the quantum Hall effect and Berry's phase in graphene," Nature **438**(7065), 201–204 (2005).
3. J. Nilsson, A. H. C. Neto, F. Guinea, and N. M. R. Peres, "Electronic properties of graphene multilayers," Phys. Rev. Lett. **97**(26), 266801 (2006).
4. A. K. Geim and K. S. Novoselov, "The rise of graphene," Nat. Mater. **6**(3), 183–191 (2007).
5. A. B. Kuzmenko, E. van Heumen, F. Carbone, and D. van der Marel, "Universal optical conductance of graphite," Phys. Rev. Lett. **100**(11), 117401 (2008).
6. R. R. Nair, P. Blake, A. N. Grigorenko, K. S. Novoselov, T. J. Booth, T. Stauber, N. M. R. Peres, and A. K. Geim, "Fine structure constant defines visual transparency of graphene," Science **320**(5881), 1308–1308 (2008).
7. S. A. Maier, *Plasmonics: Fundamentals and Applications* (Springer, 2007).
8. J. Horng, C. F. Chen, B. Geng, C. Girit, Y. Zhang, Z. Hao, H. A. Bechtel, M. Martin, A. Zettl, M. F. Crommie, Y. R. Shen, and F. Wang, "Drude conductivity of Dirac fermions in graphene," Phys. Rev. B **83**(16), 165113 (2011).
9. S. De and J. N. Coleman, "Are there fundamental limitations on the sheet resistance and transmittance of thin graphene films?" ACS Nano **4**(5), 2713–2720 (2010).
10. F. Wang, Y. Zhang, C. Tian, C. Girit, A. Zettl, M. Crommie, and Y. R. Shen, "Gate-variable optical transitions in graphene," Science **320**(5873), 206–209 (2008).
11. Y. Zhang, T. T. Tang, C. Girit, Z. Hao, M. C. Martin, A. Zettl, M. F. Crommie, Y. R. Shen, and F. Wang, "Direct observation of a widely tunable bandgap in bilayer graphene," Nature **459**(7248), 820–823 (2009).
12. L. Ju, B. Geng, J. Horng, C. Girit, M. Martin, Z. Hao, H. A. Bechtel, X. Liang, A. Zettl, Y. R. Shen, and F. Wang, "Graphene plasmonics for tunable terahertz metamaterials," Nat. Nanotechnol. **6**(10), 630–634 (2011).
13. A. Vakil and N. Engheta, "Transformation optics using graphene," Science **332**(6035), 1291–1294 (2011).
14. H. Yan, X. Li, B. Chandra, G. Tulevski, Y. Wu, M. Freitag, W. Zhu, P. Avouris, and F. Xia, "Tunable infrared plasmonic devices using graphene/insulator stacks," Nat. Nanotechnol. **7**(5), 330–334 (2012).
15. R. Alaee, M. Farhat, C. Rockstuhl, and F. Lederer, "A perfect absorber made of a graphene micro-ribbon metamaterial," Opt. Express **20**(27), 28017–28024 (2012).
16. A. Y. Nikitin, F. Guinea, F. J. Garcia-Vidal, and L. Martin-Moreno, "Surface plasmon enhanced absorption and suppressed transmission in periodic arrays of graphene ribbons," Phys. Rev. B **85**(8), 081405 (2012).
17. S. Thongrattanasiri, F. H. L. Koppens, and F. J. García de Abajo, "Complete optical absorption in periodically patterned graphene," Phys. Rev. Lett. **108**(4), 047401 (2012).

18. N. I. Landy, S. Sajuyigbe, J. J. Mock, D. R. Smith, and W. J. Padilla, "Perfect metamaterial absorber," Phys. Rev. Lett. **100**(20), 207402 (2008).
19. M. Pu, C. Hu, M. Wang, C. Huang, Z. Zhao, C. Wang, Q. Feng, and X. Luo, "Design principles for infrared wide-angle perfect absorber based on plasmonic structure," Opt. Express **19**(18), 17413–17420 (2011).
20. P. Bouchon, C. Koechlin, F. Pardo, R. Haïdar, and J.-L. Pelouard, "Wideband omnidirectional infrared absorber with a patchwork of plasmonic nanoantennas," Opt. Lett. **37**(6), 1038–1040 (2012).
21. Q. Feng, M. Pu, C. Hu, and X. Luo, "Engineering the dispersion of metamaterial surface for broadband infrared absorption," Opt. Lett. **37**(11), 2133–2135 (2012).
22. M. Pu, Q. Feng, M. Wang, C. Hu, C. Huang, X. Ma, Z. Zhao, C. Wang, and X. Luo, "Ultrathin broadband nearly perfect absorber with symmetrical coherent illumination," Opt. Express **20**(3), 2246–2254 (2012).
23. M. Pu, Q. Feng, C. Hu, and X. Luo, "Perfect absorption of light by coherently induced plasmon hybridization in ultrathin metamaterial film," Plasmonics **7**(4), 733–738 (2012).
24. J.-J. Greffet, R. Carminati, K. Joulain, J.-P. Mulet, S. Mainguy, and Y. Chen, "Coherent emission of light by thermal sources," Nature **416**(6876), 61–64 (2002).
25. M. Diem, T. Koschny, and C. M. Soukoulis, "Wide-angle perfect absorber/thermal emitter in the terahertz regime," Phys. Rev. B **79**(3), 033101 (2009).
26. X. Liu, T. Tyler, T. Starr, A. F. Starr, N. M. Jokerst, and W. J. Padilla, "Taming the blackbody with infrared metamaterials as selective thermal emitters," Phys. Rev. Lett. **107**(4), 045901 (2011).
27. J. A. Mason, S. Smith, and D. Wasserman, "Strong absorption and selective thermal emission from a midinfrared metamaterial," Appl. Phys. Lett. **98**(24), 241105 (2011).
28. A. A. Balandin, S. Ghosh, W. Bao, I. Calizo, D. Teweldebrhan, F. Miao, and C. N. Lau, "Superior thermal conductivity of single-layer graphene," Nano Lett. **8**(3), 902–907 (2008).
29. K. Kim, W. Regan, B. Geng, B. Alemán, B. M. Kessler, F. Wang, M. F. Crommie, and A. Zettl, "High-temperature stability of suspended single-layer graphene," Phys. Status Solidi **4**(11), 302–304 (2010) (RRL).
30. M. Freitag, H. Y. Chiu, M. Steiner, V. Perebeinos, and P. Avouris, "Thermal infrared emission from biased graphene," Nat. Nanotechnol. **5**(7), 497–501 (2010).
31. A. E. Miroshnichenko, S. Flach, and Y. S. Kivshar, "Fano resonances in nanoscale structures," Rev. Mod. Phys. **82**(3), 2257–2298 (2010).
32. B. Luk'yanchuk, N. I. Zheludev, S. A. Maier, N. J. Halas, P. Nordlander, H. Giessen, and C. T. Chong, "The Fano resonance in plasmonic nanostructures and metamaterials," Nat. Mater. **9**(9), 707–715 (2010).
33. M. Pu, C. Hu, C. Huang, C. Wang, Z. Zhao, Y. Wang, and X. Luo, "Investigation of Fano resonance in planar metamaterial with perturbed periodicity," Opt. Express **21**(1), 992–1001 (2013).
34. P. Del'Haye, A. Schliesser, O. Arcizet, T. Wilken, R. Holzwarth, and T. J. Kippenberg, "Optical frequency comb generation from a monolithic microresonator," Nature **450**(7173), 1214–1217 (2007).

1. Introduction

As one-atom thick carbon material described by a two-dimensional (2D) Dirac-like equation, graphene has attracted much attention in recent years with respect to its extraordinary electronic and optical properties such as ballistic transport and saturable absorption [1–4]. In the optical regime, a single sheet of homogeneous graphene has only very limited loss at Dirac point due to the extremely small thickness. The absorption is about $A \approx \pi\alpha \approx 2.3\%$, where $\alpha \approx 1/137$ is the fine structure constant [5, 6]. At lower frequencies (photon energy much smaller than the Fermi energy), the property of graphene is mainly determined by the intra-band transition which is similar to the case of Drude-type material (gold, silver, as an example) [7, 8]. The different behaviors at optical and DC conditions can be utilized to realize transparent electrodes with typical DC sheet resistances varying from a few hundred ohms per square to greater than 10^5 Ω [9].

One of the most crucial aspects of graphene is that it is optically tunable via electrostatic doping, that means, the plasmon frequency of graphene can be tuned by the chemical potential μ_c or Fermi energy E_F [10–14]. Based on the electric tunable optical properties of graphene, various applications have been proposed by different groups. For example, Feng Wang *et al*. demonstrated that sophisticated tunable terahertz metamaterials can be achieved based on graphene micro-ribbon arrays [10, 11]. At almost the same time, Nader Engheta *et al*. proposed that numerous photonic functions and metamaterial concepts can be achieved by tune the graphene conductivity [13].

More recently, researchers demonstrated that total absorption of light can be achieved by utilizing periodically patterned graphene [15–17]. Since the thickness of graphene is only one-atom thick, such enhancement of light-matter interaction is quite weird. Nevertheless, one

should note that similar absorption enhancement effect in metamaterial has already demonstrated by many groups [18–21]. The mechanism behind is believed to be the magnetic coupling between metallic patches and ground planes [19]. Also, the phase matching is of significant importance since the absorption in single sheet cannot be larger than 50% in principle [17, 22, 23].

As inspired by Kirchhoff's law, spectrally selective absorber can be used directly to control the thermal radiation, which is crucial in applications such as thermo-photovoltaics (TPV) and sub-pixel super-spectral imaging [24–27]. Likewise, one would expect that the thermal emission of graphene can be controlled in a similar way. Due to the unique thermal property of graphene such as high thermal conductivity and high temperature stability [28, 29], the thermal radiation property may be quite different from traditional metamaterial. However, the spectral and spatial control of thermal radiation in graphene system has rarely been investigated although it has been used to extract the temperature distribution and spatial location of the Dirac point in the graphene channel [30].

In this paper, we show that monolayer graphene can be used as an efficient and tunable light absorber. Rigorous transfer matrix method is utilized to calculate the reflection and absorption coefficients. It is found that multi-frequency comb-like absorption can be achieved at near grazing incidence. Based on Kirchhoff's law, the passive and active tuning of directive thermal radiation in the near-infrared frequencies is demonstrated.

2. Principle and simulation

2.1 Tunable absorption in the terahertz regime

The surface (two-dimensional) conductivity of graphene is highly dependent on the working frequency and chemical potential (or Fermi energy). When there is no external magnetic field present, the local conductivity is isotropic i.e., there is no Hall conductivity. In this case, the conductivity can be approximated for $k_B T << \mu_c, \hbar\omega$ as follows [15]:

$$\sigma_{2D}(\omega) \approx \frac{ie^2}{4\pi\hbar}\ln\left[\frac{2|\mu_c| - (\omega + i2\Gamma)\hbar}{2|\mu_c| + (\omega + i2\Gamma)\hbar}\right] + \frac{ie^2 k_B T}{\pi\hbar^2(\omega + i2\Gamma)}\left[\frac{\mu_c}{k_B T} + 2\ln(e^{-\mu_c/k_B T} + 1)\right], \quad (1)$$

where $k_B T$ is the thermal energy, μ_c is the chemical potential and Γ is the scattering rate, e, k_B, and $\hbar$ are electron charge, Boltzmann constant, and reduced Plank constant (Dirac constant), respectively. The first term in Eq. (1) is due to the contribution of inter-band transition and the second term results from intra-band transition. The frequency of transition between these two regimes is dependent on the chemical potential. The validity of Eq. (1) is checked with the help of numerical and experimental results in [5, 6, 13] for various chemical potentials. The scattering rate is assumed to be Γ = 0.43 meV. The sheet impedance of graphene can be calculated as:

$$Z_s(\omega) = \frac{1}{\sigma_{2D}(\omega)}, \quad (2)$$

which can also be transformed into traditional form by writing the 3D conductivity as $\sigma_{3D}(\omega) = \sigma_{2D}(\omega)/t$, where $t \approx 0.5$ nm is the thickness of graphene [13, 21].

As shown in Fig. 1, the proposed absorber consists of a homogeneous graphene layer and metallic layer separated by a dielectric spacer with thickness of d. The permittivity of dielectric spacer is set as 2.1. To adjust the chemical potential of graphene, a voltage can be added between the graphene and metallic ground plane. The absorbance of the absorber is then calculated using $A = 1\text{-}r^2$, where r is the reflection coefficient obtained through transfer matrix method (TMM) [19]. As shown in Fig. 2, TMM is equivalent to multiple interference

theory. Both the two methods are widely used to analyze the spectral response of multilayered structure.

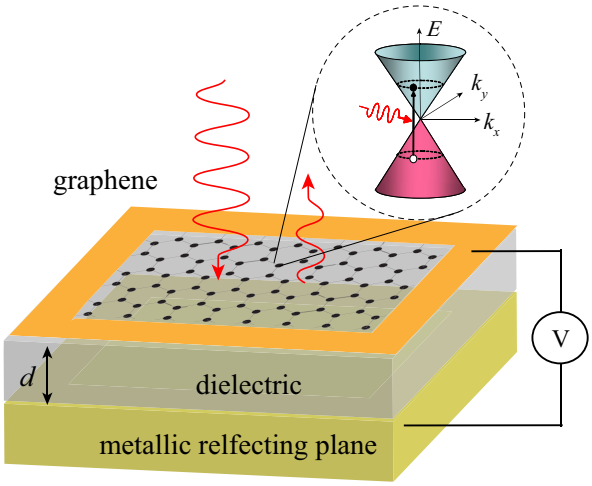

Fig. 1. Schematic of the biased graphene. The bottom gold layer is used as both the back-gate and reflecting plane to prevent transmission. Inset depicts the optical transitions between hole and electron bands in monolayer graphene.

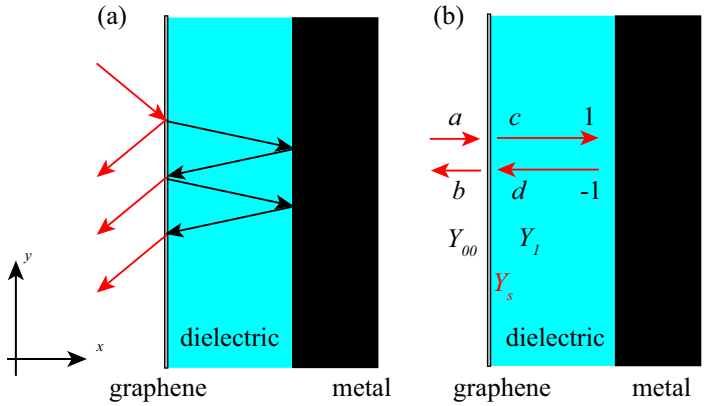

Fig. 2. Schematic of (a) multiple interference theory and (b) transfer matrix theory.

In the regime of TMM, the key of solution is the electric and magnetic boundary condition. At the two sides of the graphene, one has:

$$\begin{aligned} a+b &= e^{-ik_x d} - e^{ik_x d} \\ Y_{00}(a-b) &= Y_1(e^{-ik_x d} + e^{ik_x d}) + \frac{Z_0}{Z_s}(e^{-ik_x d} - e^{ik_x d}), \end{aligned} \tag{3}$$

where a, b, c, d are the coefficients of counter-propagating waves, Z_s is the sheet impedance of graphene, $Z_0 = 1/Y_0 = 377\ \Omega$ is the impedance of vacuum, $k_x = k_0(\varepsilon\text{-}\sin^2\theta)^{1/2}$ is the wave vector along x direction, k_0 is the wave vector in vacuum, ε is the permittivity of dielectric spacer. Y_{00} and Y_1 are the wave impedance at the left and right sides of graphene. For transverse electric (TE) polarization, there are $Y_{00} = Y_0\cos\theta$ and $Y_1 = Y_0(\varepsilon\text{-}\sin^2\theta)^{1/2}$. For transverse magnetic (TM) polarization, there are $Y_{00} = Y_0/\cos\theta$ and $Y_1 = Y_0\varepsilon(\varepsilon\text{-}\sin^2\theta)^{-1/2}$, where θ is the incidence angle.

For perfect absorption, b should be zero, thus the required sheet impedance can be written as:

$$Y_s = \frac{Z_0}{Z_s} = \cos\theta - i\sqrt{\varepsilon - \sin^2\theta}\cot(\sqrt{\varepsilon - \sin^2\theta}kd), \tag{4}$$

for TE polarization and

$$\frac{Z_0}{Z_s} = \frac{1}{\cos\theta} - i\frac{\varepsilon}{\sqrt{\varepsilon - \sin^2\theta}}\cot(\sqrt{\varepsilon - \sin^2\theta}kd), \tag{5}$$

for TM polarization.

At normal incidence, the above two required impedance can be reduced to be:

$$Z_s = \frac{Z_0}{1 - in\cot(nkd)}, \tag{6}$$

where n is the refractive index. If $Z_s = Z_0 = 377\ \Omega$, the maximal absorption condition becomes $nkd = \pi/2$, corresponding to traditional Salisbury screen (the lossy material can be either carbon or nichrome) [19].

As illustrated in Fig. 3(c), the absorbance of graphene at normal incidence for different chemical potentials is calculated using TMM. The thickness of the dielectric layer is set as 70 μm and the temperature is 300 K. For the chemical potential of 1100 meV, the maximal absorption occurs at $f = 1.36$ THz and $nkd = 2.89$. The blue shift of absorption peak can be attributed to the increase of imaginary part in graphene conductivity. As shown in Fig. 3(a) and 3(b), the imaginary parts of conductivity are much larger than the real parts ($\sigma_{2D} = 27.8 + 245i$ in units of $e^2/4\hbar$, $f = 1.36$ THz). According to Eq. (6), the large imaginary part in Z_s will make kd shift (become larger).

Compared with the Lorentzian spectra in nanostructured graphene [17], the spectrum shape becomes asymmetric, similar with the famous Fano resonance [31–33]. The asymmetric line shape stems from the fact that the absorption at 1.5 THz is always near zero for all chemical potentials. At 1.5 THz, there is $nkd = \pi$ so that the required impedance for perfect absorption becomes $Z_s = 0$, which can hardly be achieved for graphene with any chemical potential.

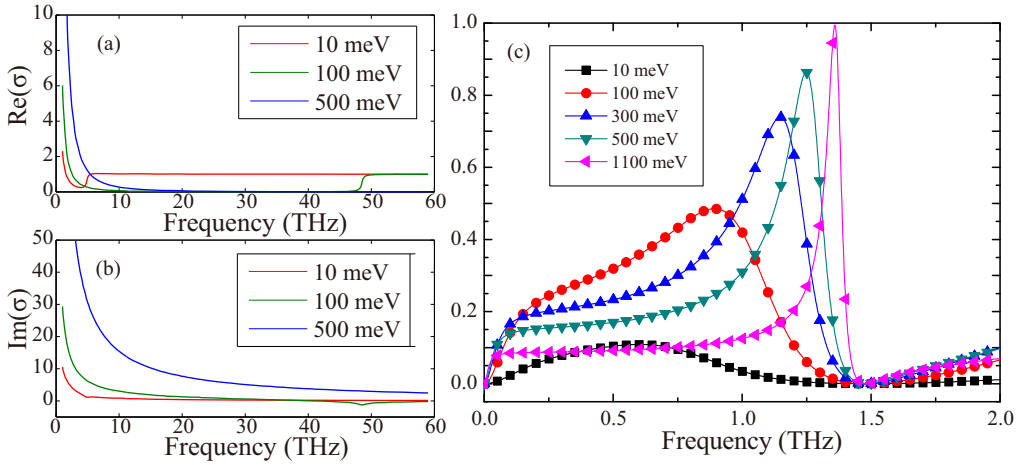

Fig. 3. (a) The real and (b) imaginary parts of graphene conductivity in units of $e^2/4\hbar$. (c) Absorbance at normal incidence for various chemical potentials.

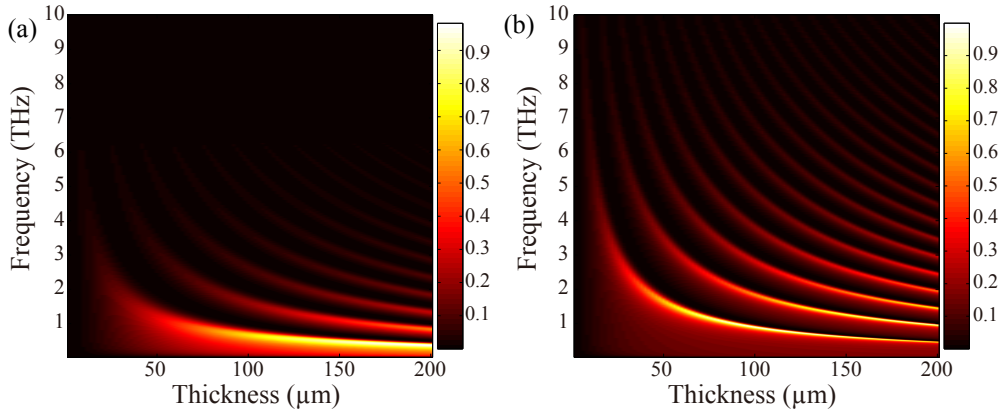

Fig. 4. Absorption as a function of the thickness of dielectric spacer and frequency for (a) μ_c = 100 meV and (b) μ_c = 500 meV.

As illustrated in Fig. 4, the thickness of dielectric spacer has great influence on the absorption. When the chemical potential increases from 100 meV to 500 meV, the required thickness for perfect absorption become decreases. Also, it can be concluded that the homogeneous graphene is not suitable for absorption at frequencies higher than 5 THz because the required chemical potential would become as high as several eV.

2.2 Absorption at large angle of incidence

In order to investigate on the angular dependence of the above structure, the absorbance for large angle of incidence is calculated for both TE and TM polarizations. The chemical potential is chosen as 200 meV and the sheet impedance at 1 THz becomes 55 + 266*i*. As illustrated Fig. 5, periodically located absorption peaks are observed for TE polarization at θ ≈83°. For TM polarization, the absorption mainly located at small angles of incidence.

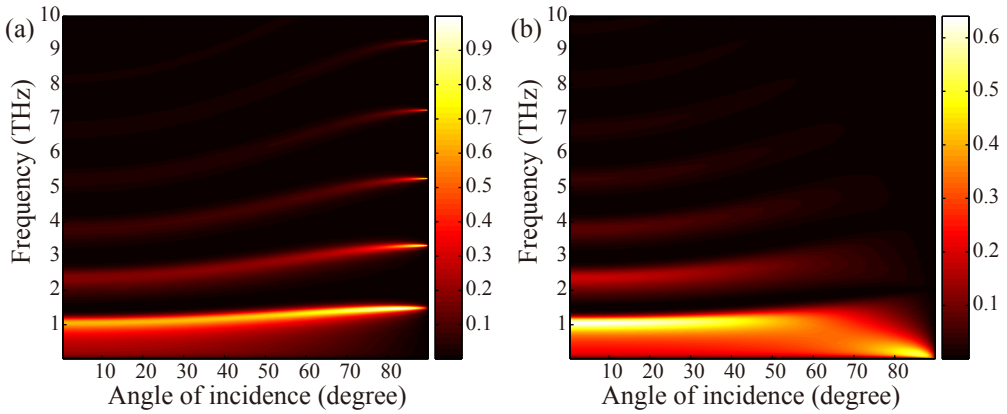

Fig. 5. (a) TE and (b) TM absorbance for different angles and frequencies. The thickness of dielectric layer is kept as 70 μm.

In order to understand the different absorption mechanism for TE and TM polarizations, the characteristics of Eqs. (4) and (5) are analyzed here.

As the impedance of graphene is larger than Z_0 for frequencies larger than 5 THz and chemical potential less than 200 meV, the prefect absorption condition (Eqs. (4) and (5)) can only be achieved when

$$kd \approx \frac{1}{\sqrt{\varepsilon - \sin^2\theta}}(\frac{\pi}{2} + m\pi). \quad \text{m=0, 1, 2, 3...} \tag{7}$$

The corresponding angles of incidence are:

$$\theta = arc\cos(\frac{Z_0}{Z_s}) = arc\cos(377\sigma_{2D}), \tag{8}$$

for TE polarization, and

$$\theta = arc\cos(\frac{Z_s}{Z_0}), \tag{9}$$

for TM polarization. It is interesting to note that the absorption angle is only dependent on the sheet impedance. Also, there is no solution for TM polarization because $Z_s > Z_0$.

According to Eq. (7), the frequency interval of adjacent absorption peaks can be written as:

$$\Delta f = \frac{c}{2d\sqrt{\varepsilon - \sin^2\theta}}. \tag{10}$$

Obviously, the permittivity of dielectric spacer has strong impact on the performance. For vacuum with $\varepsilon = 1$, Δf would be very large. As a result, the dielectric spacer provides not only mechanical support but also a phase matching for large angle of incidence.

The above discussions are only valid for the graphene-dielectric-metal sandwiched structure. In general, the structure can be extended to contain much more layers of graphene and dielectric. Just as an example, we calculated the absorption spectra when an additional dielectric cover layer with the same permittivity and thickness is added on the top of graphene. As shown in Fig. 6, periodic located absorption peaks are observed for both TE and TM polarizations. For TE polarization, the frequency intervals becomes as half of its original value, which is just the frequency interval for TM polarization. The change of frequency interval can be attributed to the interference and phase matching provided by the additional dielectric layer.

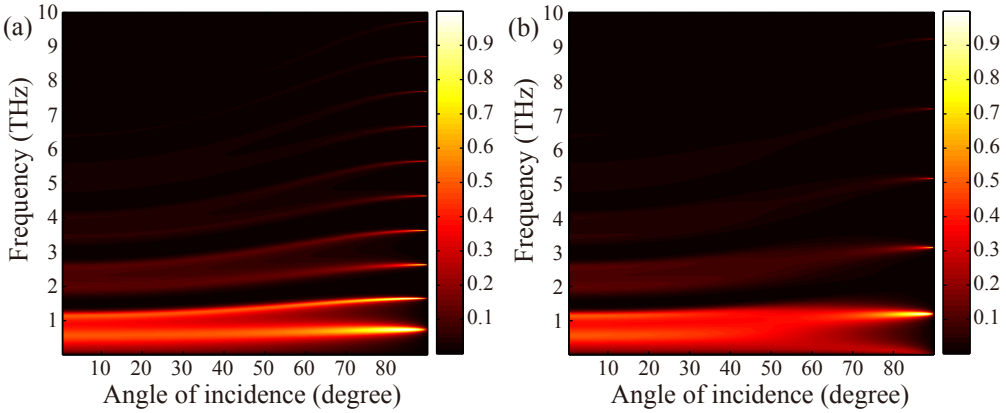

Fig. 6. (a) TE and (b) TM absorbance for single layer graphene with an additional cover layer. The thickness of dielectric layer is 70 μm.

2.3 Thermal radiation engineering

According to Kirchhoff's law of thermal radiation, at equilibrium condition the emissivity of a material equals its absorptivity [24–27]. Since graphene possess exotic optical and thermal

properties, it provides an ideal platform for the engineering of thermal radiation. In particular, the multi-frequency comb-like behavior of the graphene absorption spectra can be utilized to generate frequency comb, which has been realized by various approaches [34]. The polarization of the radiation can be tuned by the cover layer. In the following, we will only consider the case without additional cover layer.

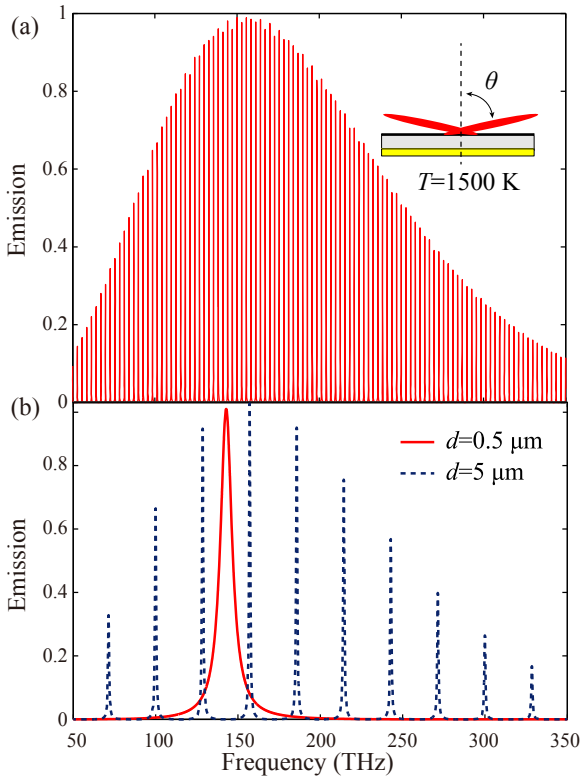

Fig. 7. (a) TE-polarized thermal emission of the graphene structure at $\theta = 88.5°$ and $T = 1500$ K for $d = 50$ μm. Inset is the schematic of the radiation pattern. (b) TE-polarized emission spectra for $d = 0.5$ μm and 5 μm.

At near-infrared and visible frequencies, the conductivity of monolayer graphene ($\mu_c = 0$) becomes a universal constant equal to $e^2/4\hbar$, which can be obtained from the asymptotic behavior of Eq. (1). As proved in [10], the optical conductivity is weakly dependent on the working temperature. The optical sheet resistance can be calculated as 16.4 KΩ. In numerical simulations, the emission of metal backed graphene is calculated by the product of emissivity (absorbance) and the blackbody radiation. As an example, the temperature is set as 1500 K and the corresponding radiation center frequency is 155.44 THz ($\lambda = 1.93$ μm). The radiation angle is then calculated to be $\theta = 88.5°$. Since the absorption at $\theta = 0°$, 30°, and 60° is only 0.09, 0.1, 0.17 for TE polarization (the case for TM polarization is even smaller), the emissivity is highly dependent on the angle.

Due to the strong angle dependence of the thermal radiation, it can be utilized as highly directive thermal source. According to Eq. (10), the thickness of the dielectric layer can be changed to achieve different kinds of radiation property such as narrow band single peak radiation (small d) or multi-frequency comb-like radiation (large d). As illustrated in Fig. 7, the thermal emissions of the structure for different dielectric thicknesses are calculated. When the thickness of dielectric layer is set as 50 μm, 5 μm, and 0.5 μm, the corresponding

frequency interval between adjacent peaks becomes 2.86 THz, 28.6 THz and 286 THz, respectively.

The thermal radiation property can also be adjusted by the chemical potential. As the increase of μ_c, the inter-band transition shift to higher frequency. Due to the abrupt change of conductivity, the emission spectrum will also experience a rapid alteration. The conductivities and emission spectra ($\theta = 88.5°$) for $\mu_c = 200$ meV and 300 meV are illustrated in Fig. 8. Here the thickness of the dielectric spacer is kept as 10 μm. Obviously, the emission spectra at frequency higher than $2\mu_c/h$ are not changed by the chemical potential while the emission at lower frequencies is completely suppressed.

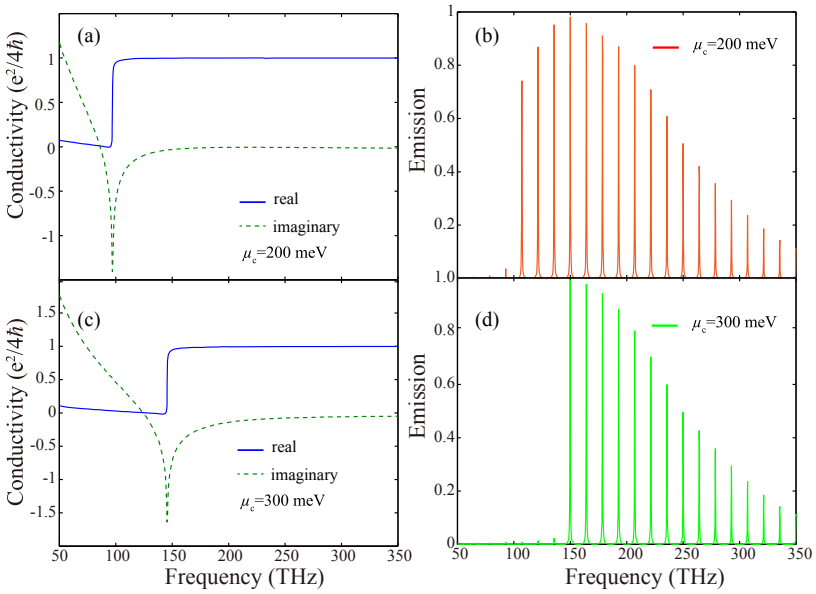

Fig. 8. (a) (b) Conductivity and corresponding emission spectrum of graphene for μ_c = 200 meV and d = 10 μm. (c)(d) The conductivity and emission for μ_c = 300 meV.

The above discussion is limited for monolayer graphene. In fact, the radiation angle can be changed by layer number of multilayer graphene. Since the optical conductivity is in proportional with the layer number [5, 6], the conductivity of bilayer and trilayer graphene would be twice and triple of $e^2/4\hbar$. In Fig. 9, the radiation patterns at f = 155 THz (d = 0.46 μm) for 1, 5, and 10 layers of graphene are calculated using transfer matrix method for different radiation angles. As the increase of the layer number, the radiation angle will decrease according to Eq. (8). Meanwhile, the radiation at small angle (such as normal direction) will increase and the beam width would be larger. Thus for practical applications, a trade-off between radiation angle and beam width is required.

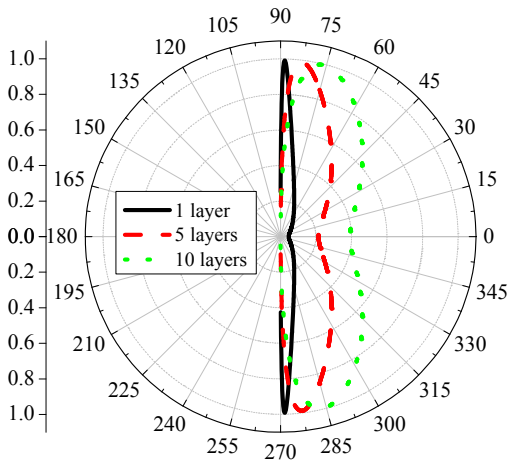

Fig. 9. Polar plot of the radiation pattern of graphene with 1, 5, and 10 layers. The sample is placed vertically and the radiation angles are ranging from 0° ~90° and 270° ~360°.

Finally, we would like to comment that the thermal radiation of graphene can hardly be achieved using traditional metal film. For example, the conductivity of nichrome at 150 THz is about 1e5 S/m [21], thus a thickness of 0.6 nm would be required for the same sheet resistance (16.4 KΩ). Although material with smaller conductivity seems a possible solution, the requirement for thermal property may not be fulfilled as the temperature should be so high.

Conclusion

In summary, we proposed a high efficient electromagnetic absorber based on monolayer graphene. It is demonstrated numerically that the terahertz absorbance in graphene can be dynamically tuned by the chemical potential. Moreover, a set of periodically located absorption peaks at near grazing incidence is observed. The polarization and angle dependences of the absorption are analyzed carefully. Finally, a thermal radiator with tailored radiation pattern is demonstrated by utilizing the universal constant conductivity of graphene at near infrared frequencies.

Acknowledgments

This work was supported by 973 Program of China (No. 2013CBA01700), National Natural Science Funds (No. 61138002) and Chinese Academy of Sciences for Graduate Innovative Research.